Available online at www.sciencedirect.com
ScienceDirect
Journal of Sound and Vibration 321 (2009) 537–553
JOURNAL OF SOUND AND VIBRATION
www.elsevier.com/locate/jsvi

# Performance enhancement of pneumatic vibration isolation tables in low frequency range by time delay control

Yun-Ho Shin, Kwang-Joon Kim*

*Center for NOVIC, Department of Mechanical Engineering, KAIST, Science Town, Daejeon 305-701, South Korea*

Received 4 August 2008; received in revised form 10 October 2008; accepted 25 October 2008
Handling Editor: J. Lam
Available online 9 January 2009

**Abstract**

As environmental vibration requirements on precision equipment become more stringent, the use of pneumatic isolators has become more popular and their performance is subsequently required to be further improved. Dynamic performance of passive pneumatic isolators is related to various design parameters in a complicated manner and that in low-frequency range is limited by resonance frequency or volume of pneumatic chambers in practice.

In this study, an active control technique, called as time delay control, is applied to a pneumatic isolator to enhance the isolation performance in the low frequency range where the passive techniques have difficulties. This time delay control technique is taken especially because it is known to be useful for the low frequency control. The procedure of applying the time delay control technique to the pneumatic isolator is presented, together with how to resolve distortion problems in actuator dynamics in implementing the active control technique into a pneumatic system. Effectiveness of the technique in enhancement of transmissibility performance is shown based on simulation as well as experiments. Comparisons with passive pneumatic isolators are also presented.


## 1. Introduction

Precision instruments such as steppers (for processing of semiconductors), electron-beam microscopes and laser systems are highly sensitive to ground or environmental vibrations. As higher precision or resolution is needed, requirements on the ground vibration level have become more stringent in regulations or standards [1]. Thus, as a solution, pneumatic isolators are often used to isolate vibrations from the ground.

It is well known that pneumatic vibration isolation tables yield good performance at excitation frequencies fairly above the natural frequencies of the system and become deteriorated as the excitation frequency gets close to those, which are typically 2–6 Hz. Recently, standards for ground vibrations in the frequency range lower than 10 Hz have become tougher [1], asking for further reduction of natural frequencies of the vibration isolation tables through design modifications. Because, however, the resonance frequencies in the passive isolation technique are inherently determined by the payload and the volume of pneumatic chamber [2,3],

*Corresponding author. Tel.: +82 42 350 3024; fax: +82 42 350 8220.
*E-mail address:* kjkim@kaist.ac.kr (K.-J. Kim).

0022-460X/$ - see front matter © 2008 Elsevier Ltd. All rights reserved.
doi:10.1016/j.jsv.2008.10.030

**Nomenclature**

| | |
|---|---|
| $\mathbf{A_m}$ | desired system matrix for time delay control |
| $\mathbf{B_m}$ | command distribution matrix |
| $\mathbf{B_c}$ | distribution matrix of the control input |
| $A$ | area ($m^2$) |
| $F$ | force (N) |
| $G$ | frequency response function |
| $K_p$ | proportional control gain |
| $K_d$ | derivative control gain |
| $R$ | the universal gas constant ($=286.9$ (J/(kg K))) |
| $T$ | temperature (K) |
| $V$ | volume ($m^3$) |
| $\mathbf{d}$ | unknown disturbance vector |
| $\mathbf{u}$ | control input vector |
| $\mathbf{x}$ | system state vector |
| $\mathbf{f}$ | unknown dynamics of plant |
| $\mathbf{r}$ | command vector |
| $a$ | coefficient of modified integrator |
| $b_c$ | second column element of $\mathbf{B_c}$ |
| $c$ | viscous damping |
| $d$ | desired pressure |
| $e$ | error |
| $k$ | stiffness (N/m) |
| $p$, $P$ | pressure ($N/m^2$) |
| $t$ | time (s) |
| $u$ | control input |
| $x$ | displacement (m) |
| $m$ | payload (kg) |
| $\Delta$ | difference |
| $\kappa$ | the specific heat ratio |
| $\rho$ | density ($kg/m^3$) |
| $\mu$ | dynamic viscosity ($N\,s/m^2$) |
| $\omega$ | excitation frequency (rad/s) |
| $\varsigma$ | damping ratio |
| $j$ | square root of $-1$ |
| $L$ | delay time (s) |

*Subscripts*

| | |
|---|---|
| $B$ | vibration on base |
| $D$ | desired-pressure |
| $P$ | measured-pressure |
| $V$ | voltage |
| $X$ | vibration on payload |
| $d$ | diaphragm |
| $b$ | base |
| $c$ | control |
| $d$ | diaphragm |
| $p$ | payload |
| $s$ | single chamber |
| 0 | static |
| exp | experiment |
| th | theoretical |
| max | maximum |

*Superscripts*

| | |
|---|---|
| $\wedge$ | estimation |
| $+$ | pseudo-inverse |
| . | first derivative with respect to time |
| * | complex variable |

natural frequencies cannot be lowered endlessly. Therefore, as a solution to overcome this difficulty in the low frequency excitation, one active technique called time delay control (TDC) technique is chosen in this study to control the pressure inside the pneumatic chamber.

Pneumatic vibration isolators mostly work under heavy static payload while dynamic loading superposed to the static one is typically very small. Because commercial sensors for measurement of both large static pressure and extremely small dynamic pressure are available only recently, there are not many publications on active control of pneumatic pressure. Particularly, there exist few researches on the active pressure control of pneumatic vibration isolators pertaining to the ground excitation.

Oshio [4] may be the first who made a study on an active pneumatic vibration isolator for ground vibrations using pole-placement method in the 1990s. He focused on the movement of a system pole, i.e., natural frequency and damping ratio. Recently, Shih [5] used an adaptive and fuzzy controller for the ground vibration problem. The method, known to be good for nonlinear or time-varying system, may not be easy to design and apply in practice. Kawashima [6] worked on the ground vibration as well using a PID control technique by focusing on the sensing of dynamic pressure. In several other studies [7–9], how to reduce the settling time in case of the payload excitation by pneumatic control were proposed.

In the present study, a methodology to enhance the performance of a pneumatic vibration isolator for ground excitations by controlling dynamically the air pressure inside pneumatic chamber is proposed based on

so called TDC technique [10–12]. The TDC technique is considered to be simple, robust and, hence, easily applicable to real world systems, which may behave in either linear or nonlinear ways [10–12].

The procedure of applying the TDC technique to the pneumatic isolator is presented and its effectiveness in enhancement of transmissibility is shown based on simulation and experimental studies. A key problem here is to control the pressure of air dynamically inside the chamber subject to a high static pressure by using a pneumatic valve as an actuating component. Although the valve alone makes the air flow rate proportional to the input voltage, the actuator system consisting of the valve, the tube, and the chamber does not necessarily behave in a simple manner. How to resolve this problem by both feedforward and feedback control is also addressed. How much enhancement could be obtained by the active technique is shown by comparing with the performance by the purely passive isolator.

## 2. Bases for application of TDC technique to pneumatic vibration isolator

Mathematical modeling of the pneumatic isolator was discussed in Ref. [2] and detailed dynamic characteristics of the pneumatic isolator such as the amplitude dependent stiffness due to the rubber diaphragm were discovered via actual measurements [3,13]. However, it is not easy to derive a nonlinear mathematical model in time domain from nonlinear behaviors observed in frequency domain for the purpose of active control. It is known that the TDC technique is an excellent tool for a system whose accurate model is not easy to obtain, because this technique employs a reference model and the control algorithm makes the system follow the reference model somehow. The TDC technique, however, requires all state variables; displacement, velocity and acceleration and is especially useful for systems of slow response characteristics, because it calculates the control input by estimating approximately current states simply from those just a few sampling times ago.

Since a single chamber pneumatic spring can be a basis of many other types of pneumatic isolators, state equation for vertical movement of a system consisting of single chamber pneumatic spring and a payload is formulated. The procedure to design and apply the TDC is explained in this section and its effectiveness is shown by the simulations.

### 2.1. Derivation of state equation

Consider a pneumatic vibration isolation system consisting of a payload and a single pneumatic chamber as shown in Fig. 1. Stiffness of the single chamber is known to be dependent on frequency and amplitude of

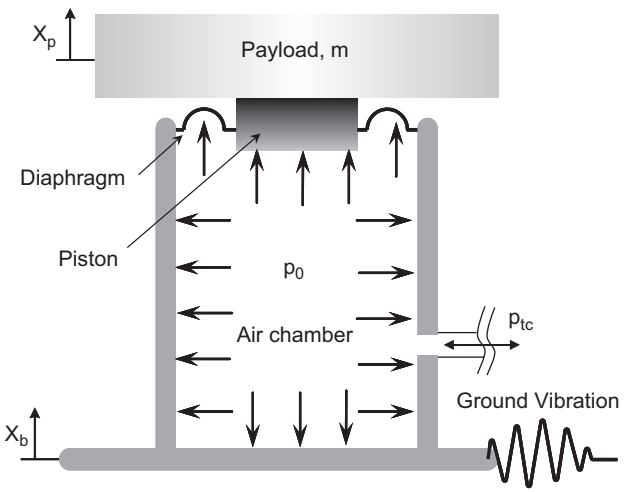


Fig. 1. Schematic diagram of pneumatic vibration isolator with payload on it for excitation at ground.

Table 1
Parameters of pneumatic spring and payload.

| Symbol | Name | Value |
|---|---|---|
| $m$ | Payload | 87 kg |
| $\rho$ | Density | 5.97 kg/m$^3$ |
| $\mu$ | Dynamic viscosity | $1.79\times10^{-5}$ N s/m$^2$ |
| $R$ | Gas constant | 286.9 J/(kg K) |
| $\kappa$ | Specific heat ratio | 1.4 |
| $T_0$ | Temperature | 288.1 K |
| $P_0$ | Static pressure | $3.51\times10^5$ Pa |
| $V$ | Chamber volume | $2.978\times10^{-4}$ m$^3$ |
| $A_p$ | Effective piston area | $2.518\times10^{-3}$ m$^2$ |
| $c_d$ | Equivalent viscous damping of diaphragm | $2.87\times10^2$ N s/m |
| $k_d$ | Real part of complex stiffness of diaphragm | $1.12\times10^4$ N/m |

vibration [3,13] and, hence, can be expressed as such, $k^*(X_p,\omega)$,

$$k^*(X_p,\omega)=k_s+k_d^*(X_p,\omega), \tag{1}$$

where $k_s$ denotes real stiffness of the single chamber given by $\kappa p_0 A_p^2/V_{t0}$ [2], $k_d^*$ complex stiffness of rubber diaphragm used for sealing. The complex stiffness of the rubber diaphragm, which is amplitude and frequency dependent [13], is very hard to model by a mathematical equation. The mean value of measurements of the complex stiffness has been taken in this study for simplicity in the simulation.

The equation of motion for pneumatic vibration isolation table in Fig. 1 can be written as:

$$m\ddot{x}_p+c_d(\dot{x}_p-\dot{x}_b)+(k_s+k_d)(x_p-x_b)=A_p p_{tc}, \tag{2}$$

where $m$ denotes the mass of payload (87 kg), $k_d$ and $c_d$ denote real part of the complex stiffness of diaphragm ($1.12\times10^4$ N/m) and equivalent viscous damping of diaphragm ($2.87\times10^2$ N s/m), $A_p$ effective area of the piston to represent both cross-sectional area of the piston and movement of the diaphragm [2,3], $p_{tc}$ dynamic pressure supplied into the chamber through the actuator which will be dealt in Section 2.2 in detail.

Eq. (2) enables the state equation to be written as follows:

$$\begin{bmatrix}\dot{x}_p\\ \ddot{x}_p\end{bmatrix}=\begin{bmatrix}0 & 1\\ -\dfrac{k_s+k_d}{m} & -\dfrac{c_d}{m}\end{bmatrix}\begin{bmatrix}x_p\\ \dot{x}_p\end{bmatrix}+\begin{bmatrix}0\\ \dfrac{1}{m}\end{bmatrix}[(k_s+k_d)x_b+c_d\dot{x}_b]+\begin{bmatrix}0\\ \dfrac{A_p}{m}\end{bmatrix}p_{tc}, \tag{3}$$

where the second and third terms on the right-hand side denotes ground vibration, control input, respectively. Values of each parameter for the pneumatic spring and payload are described in Table 1.

### 2.2. Simulation for pneumatic vibration isolator with TDC

#### 2.2.1. TDC law

Let us consider a system, which can be either time invariant linear or time varying linear, or nonlinear to be more general, described by

$$\dot{\mathbf{x}}(t)=\mathbf{f}(\mathbf{x},t)+\mathbf{B_c}(\mathbf{x},t)\mathbf{u}(t)+\mathbf{d}(t), \tag{4}$$

where $\mathbf{x}$ represents state vector of the underlying system, $\mathbf{f}(\mathbf{x},t)$ dynamics of the plant, $\mathbf{B_c}(\mathbf{x},t)$ distribution matrix of the control input vector $\mathbf{u}(t)$, and $\mathbf{d}(t)$ unknown disturbance vector. In the TDC technique, all state variables and their first time derivatives are assumed available and a reference model with desirable dynamic characteristics, e.g., natural frequency and damping ratio is chosen for the underlying system, which must be linear and time-invariant as described below:

$$\dot{\mathbf{x}}_\mathbf{m}(t)=\mathbf{A_m}\mathbf{x_m}(t)+\mathbf{B_m}\mathbf{r}(t), \tag{5}$$

where $\mathbf{x_m}(t)$ denotes state vector of the reference model, $\mathbf{A_m}$ the system matrix, $\mathbf{B_m}$ command distribution matrix, and $\mathbf{r}(t)$ command vector. The control input $\mathbf{u}(t)$ to the system is determined such that the plant in Eq. (4) keep track the reference model in Eq. (5) as close as possible, i.e., such that the difference between plant and reference model be minimized, as follows:

$$\mathbf{u}(t) = \hat{\mathbf{B}}_\mathbf{c}^{+}[-\hat{\mathbf{f}}(\mathbf{x},t) - \mathbf{d}(t) + \mathbf{A_m}\mathbf{x}(t) + \mathbf{B_m}\mathbf{r}(t)]. \tag{6}$$

In Eq. (6), $\hat{\mathbf{B}}_\mathbf{c}^{+}$ denotes the pseudo-inverse of $\hat{\mathbf{B}}_\mathbf{c}$, which is a constant matrix representing a known range of $\mathbf{B_c}(\mathbf{x},t)$ and $\hat{\mathbf{f}}(\mathbf{x},t)$ denotes the unknown plant dynamics. Note here that the control input $\mathbf{u}(t)$ can be determined only if $\hat{\mathbf{f}}(\mathbf{x},t) + \mathbf{d}(t)$ is available. When the actual system and the disturbance have slow dynamic characteristics, $\hat{\mathbf{f}}(\mathbf{x},t) + \mathbf{d}(t)$ can be replaced approximately with $\hat{\mathbf{f}}(\mathbf{x},t-L) + \mathbf{d}(t-L)$, where $L$ is a time delay very small relative to the time characteristics of the system, as shown below:

$$\hat{\mathbf{f}}(\mathbf{x},t) + \mathbf{d}(t) = \dot{\mathbf{x}}(t) - \hat{\mathbf{B}}_\mathbf{c}\mathbf{u}(t) \cong \dot{x}(t-L) - \hat{\mathbf{B}}_\mathbf{c}\mathbf{u}(t-L). \tag{7}$$

The small time delay $L$ can be an integer multiples of the sampling time in discrete time control. By substituting Eq. (7) into Eq. (6), the control input is derived as follows:

$$\mathbf{u}(t) = \mathbf{u}(t-L) + \hat{\mathbf{B}}_\mathbf{c}^{+}[-\dot{\mathbf{x}}(t-L) + \mathbf{A_m}\mathbf{x} + \mathbf{B_m}\mathbf{r}]. \tag{8}$$

Each term in Eq. (8) to compute the control input will be explained or designed in more detail in Section 2.2.2. The most important requirement in this TDC technique is that values of all the state variables and their first derivatives must be provided by some means, which will be addressed in Section 3.1. As can be seen in a block diagram for the TDC in Fig. 2, the control input consists of two parts; the first part canceling the unknown dynamics and the disturbance by using the time delay $L$ and the second part adding the desired trajectory and the reference model dynamics.

### 2.2.2. Simulation results of pneumatic vibration isolator by TDC

By combining Eqs. (3) and (8), the control input pressure can be determined as follows:

$$u(t) = p_{tc}(t) = p_{tc}(t-L) + \mathbf{B}_\mathbf{c}^{+}[-\dot{\mathbf{x}}_\mathbf{p}(t-L) + \mathbf{A_m}\mathbf{x_p}(t)],$$

$$\mathbf{x_p} = \begin{bmatrix} x_p \\ \dot{x}_p \end{bmatrix}, \quad \mathbf{B}_\mathbf{c}^{+} = [0 \quad m/A_p],$$

$$A_m = \begin{bmatrix} 0 & 1 \\ -\omega_n^2 & -2\varsigma\omega_n \end{bmatrix}. \tag{9}$$

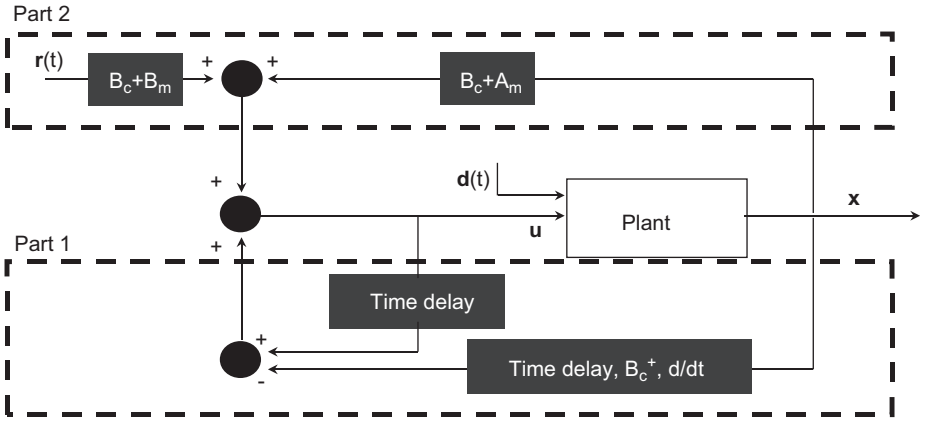


Fig. 2. Block diagram of time delay controller.

Comparing Eq. (9) with Eq. (8), state vector of the plant and its derivative shows up together with characteristics of the reference model while the command terms $r(t)$ are set to zero. The reference model described by the matrix $\mathbf{A_m}$ is a target system which has to be achieved by the TDC control. Therefore, the matrix $\mathbf{A_m}$, consisting of a natural frequency and a damping ratio in this case, need to be designed or selected carefully. To enhance the isolation performance of the pneumatic table against the ground vibration, the natural frequency of the reference model should be as small as possible compared with that of the actual plant and a certain amount of damping is necessary to limit the vibration level at the resonance. In this study, the natural frequency of the reference model was chosen as 0.5 Hz by considering the resonance frequency of the plant around 3 Hz and the useful frequency range ($>0.5$ Hz) of the acceleration sensor used in the experimental measurement. The damping was simply chosen as the critical ($\varsigma = 1$). The time delay, $L$, was set as the sampling time (0.001 s), which is far smaller than the system's natural period after control 2 s. Theoretical range of the tuning parameter $b_c^+$ in the TDC technique [10–12], which corresponds to the second element of $\mathbf{B_c^+}$ in Eq. (9), for the stability and the uncertainty, is given by the payload m divided by the effective area of piston $A_p$ as follows:

$$0 < b_{c\,\mathrm{th}}^{+} < 39714 (= m/A_p). \tag{10}$$

In simulation, the tuning parameter $b_c^+$ was chosen as maximum value 39714($= m/A_p$) because a larger value is desirable as long as the system is stable. The stable range and the value in experimental active control will be dealt with in Section 3.3.

A simulation study is accomplished under a random ground vibration condition of 30 $\mu m/s_{rms}$, which, corresponding to the criteria VC-C in standard of ground vibration [1], is a vibration level allowed marginally for electron microscopes. Parameters of the air spring and the payload described in Table 1 were used for the simulation, which were obtained from experimental works. In order to see the isolation performance, vibration signals at the payload were calculated for the excitations given at the base and the transmissibility was estimated from the two signals as follows:

$$\text{Transmissibility} = \frac{G_{BX}}{G_{BB}}, \tag{11}$$

where the subscripts $B$ and $X$ denote the vibration signals at the base and on the payload, respectively, $G_{BX}$ and $G_{BB}$ cross- and auto-power spectral density function, respectively [14]. The transmissibility function was estimated from the random signals by applying Hanning window, by ensemble average of 50 times, and at a frequency resolution of 0.2 Hz. The results in Fig. 3 show that the isolation performance of the active pneumatic isolator based on the TDC technique is far better than that of the passive one as expected. The mean value of the transmissibilities by the TDC is less than 1% of that by the passive one. The transmissibility obtained by the active TDC shows almost exactly the dynamics of the reference model described by the

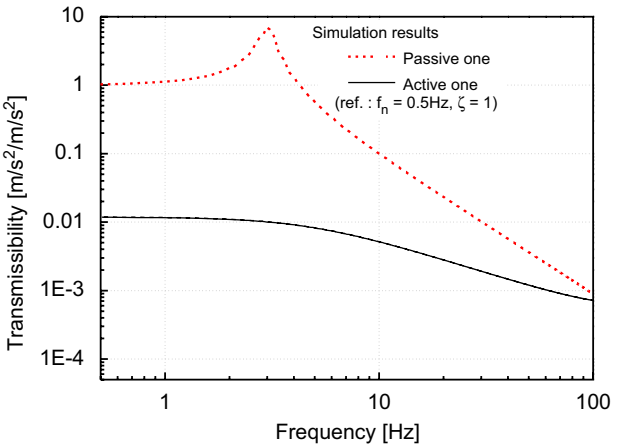


Fig. 3. Simulation results of passive- and active-pneumatic vibration isolator.

natural frequency of 0.5 Hz and critical damping ratio $\zeta = 1$. However, transmissibility of the actual active isolator can be distorted by several factors such as dynamic characteristics of the actual actuator, signal filtering and imperfect measure of all states. Further details will be treated in Section 3.3.

## 3. Experimental active control of pneumatic table by TDC

Procedures of experimental works for active control of pneumatic vibration isolation table by the TDC technique are first discussed in this section. A proportional valve of nozzle-flapper type (Model: Moog J814-0005) was used to control the dynamic pressure in the pneumatic chamber. In preliminary investigations, significant time lag was observed between command input into the valve and variation of pressure in the chamber, which caused poor pressure control inside the chamber. Therefore, relationship between dynamic voltage input to the valve and dynamic pressure output in the chamber was examined very carefully. Feedforward and feedback control techniques were introduced into the pneumatic actuator to counteract the time delay and possible instability in the actuator itself.

Experimental results obtained by applying the TDC technique and pneumatic actuator with internal compensation mechanisms are presented and compared with those by the passive technique. Effectiveness of the active TDC technique for a pneumatic vibration isolation table is illustrated in terms of very low values of transmissibility, especially, over a low frequency range ($<10$ Hz) where passive technique yields high values.

### 3.1. Experimental set-up for application of TDC technique

Fig. 4 shows a schematic diagram of the actively controlled pneumatic vibration isolation table with a payload on it together with a photograph for the whole system. The air pressure inside the chamber, which works as a spring, is directly controlled by the valve actuation, which is the key concept in this study to counteract the disturbances from the ground.

The voltage (V) into the pneumatic valve and the pressure in chamber ($p_{tc}$) to be controlled are processed by dSPACE ControlDesk and Simulink of MatLab in a personal computer. The voltage calculated in the computer is supplied to the valve by dSPACE Model ds1103 and the measured pressure and acceleration signals are digitized also by the ds1103. The valve works not only to maintain a static pressure

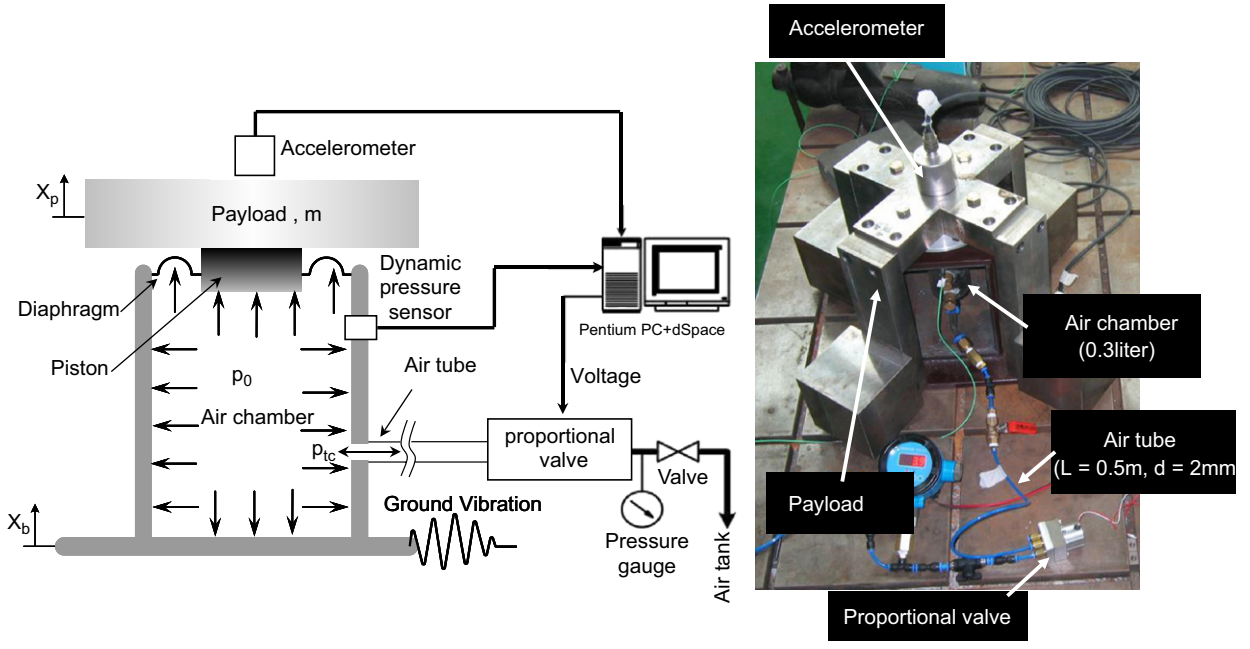


Fig. 4. Experimental set-up and diagram of TDC applied pneumatic isolation table with payload.

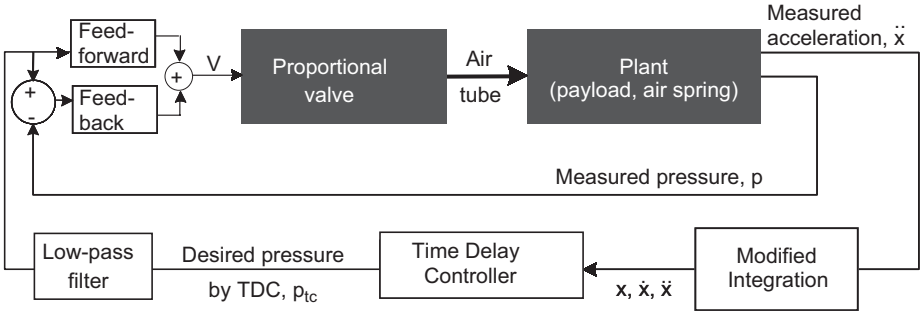


Fig. 5. Block diagram of time delay controlled pneumatic vibration isolation system.

$p_0 = 3.5 \times 10^5$ Pa but also to supply the required dynamic pressure. A high precision dynamic pressure sensor (Model: PCB 106B, sensitivity: 43 mV/kPa) was installed into the chamber and a highly sensitive seismic accelerometer (Model: PCB 393B05, sensitivity: 10 V/g) was fixed on the payload, weight of which is 87 kg. The payload for the single spring was chosen as one-fourth of the full payload which is supported by four pneumatic springs of the same type in a commercial model. The shape of payload for the single spring was chosen as shown in photograph of Fig. 4, so that its mass center was positioned lower than the connection point with the air spring, to reduce unstable tilting motions. The pneumatic spring is composed of a single chamber, a rubber diaphragm and a piston. Two holes were drilled through the chamber wall; one for installation of the dynamic pressure sensor and the other for supply of the control pressure.

A block diagram for the whole closed-loop system is shown in Fig. 5, where the plant consists of the payload and the pneumatic spring. Since just acceleration was measured on the payload while the TDC technique requires full state vector, it was necessary to estimate the velocity and displacement by numerical integrations. A method called modified integration was employed to calculate velocity and displacement from the acceleration. Both feedforward and feedback controllers were used to compensate for distortion caused by the valve dynamic and the tube characteristics between the valve and the chamber. Detailed explanations of this problem are given in Section 3.2.

As mentioned above, all states composed of displacement, velocity and acceleration of the payload must be available in the TDC technique. Since, however, often only the acceleration is measured on the payload due to convenience of measurement, numerical integrator or other state estimator must be used to obtain the velocity and displacement of the payload. Use of the ideal integration method accumulates even a small DC offset value measured by the acceleration sensor while a modified integration [15] can remove the accumulation of the DC offset. The modified integrator is just a slight variation of the ideal integrator as shown below:

$$\frac{1}{s} \to \frac{1}{s+a}, \tag{12}$$

where $s$ is Laplace operator. The modified integrator is a first-order system with cut-off frequency, $a$. The parameter '$a$' affects distortion of the phase of the signal as well as extent of accumulation of the DC offset. As a rule of thumb [15], the value of '$a$' is chosen as about $\frac{1}{10}$ of the lower limit of frequency range of interest. In this study, 0.5 Hz was chosen.

A low pass filter was employed to eliminate the measurement noise and to guarantee the isolation performance of passive pneumatic spring above the frequency range of interest (10 Hz). It was a second-order IIR filter (Butterworth) [16] with cut-off frequency at 40 Hz, which was chosen by considering the main frequency range of interest.

### 3.2. Dynamic pressure control by valve actuation

#### 3.2.1. Frequency response characteristics between voltage to valve and pressure in chamber without any control

A pneumatic 'proportional' valve of nozzle-flapper type (Model: Moog J814-0005) was used to control the air pressure inside the pneumatic chamber. The static relationship between the input voltage supplied to the

valve and the pressure in the chamber was almost linear, i.e., proportional and the slope or sensitivity was obtained by curve fitting as $3.19 \times 10^4$ Pa/V with root mean square error of 0.9% over the operating voltage range 0–5 V. The above results were obtained by measuring the pressures in the pneumatic chamber 5 min after every step input of voltage by 0.2 V from 0–5 V. A digital pressure gauge (model: Sensys SMG, range: −0.9 to 9 bar) was used to measure the static pressure and commands to the valve of the static voltage supply were controlled by the personal computer.

Dynamic characteristics of the actuator, which must be essentially known for a successful active control of dynamic pressure in the chamber over a few Pascals, were identified under a high static pressure of $3.5 \times 10^5$ Pa. A schematic diagram of the experimental set-up to measure frequency response characteristics of the pneumatic actuator is shown in Fig. 6. The random voltage generated by dSPACE Model ds1103 and PC (dSPACE ControlDesk & Simulink in MatLab) was supplied to the valve, which was connected to the pneumatic chamber of volume $0.3 \times 10^{-3}$ m$^3$ through an air tube of length 0.5 m and diameter 0.002 m. The properties of air and parameters of the spring are given in Table 1. The pressure of air supplied to the proportional valve was $5.0 \times 10^5$ Pa and the static pressure in the chamber, which was determined by static position of the flapper in the valve [17], was maintained at $3.5 \times 10^5$ Pa. A high-precision dynamic pressure sensor (model: PCB 106B, sensitivity: 43 mV/kPa) was installed into the chamber wall to measure the dynamic pressure passing. The voltage and dynamic pressure signals were processed to compute the frequency response function $\mathrm{FRF}_{VP}$ as described below:

$$\mathrm{FRF}_{VP} = \frac{G_{VP}}{G_{VV}}, \tag{13}$$

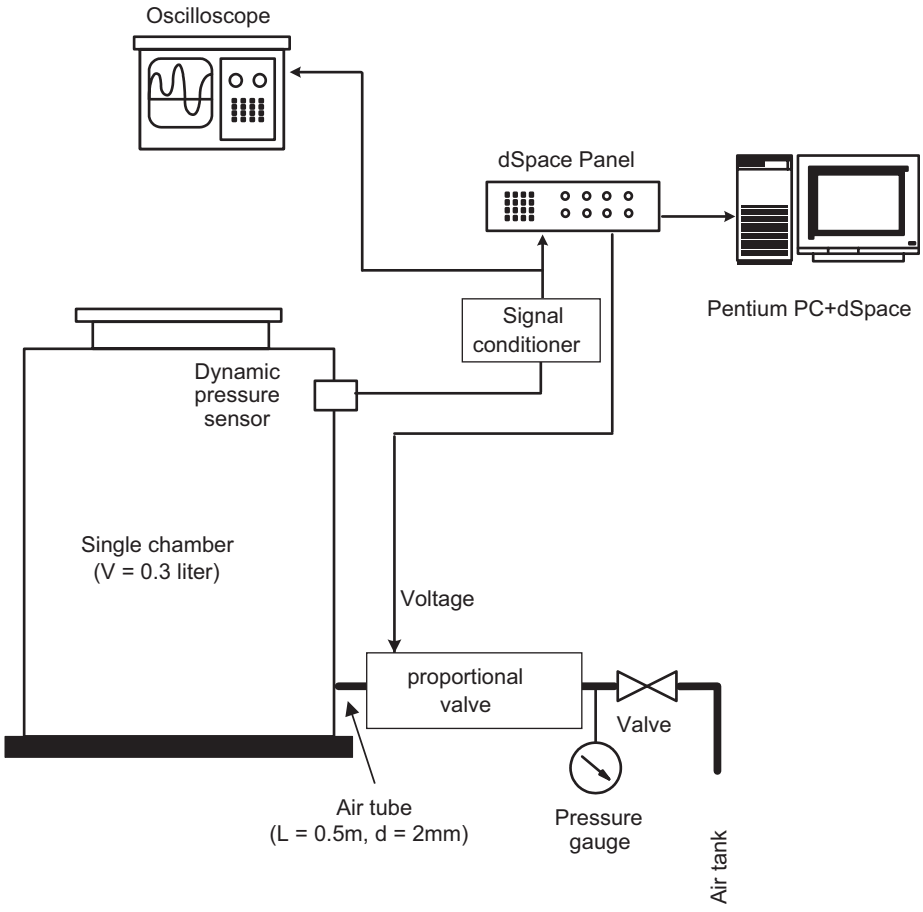


Fig. 6. Experimental set-up and block diagram for measurement of dynamic response characteristics of pressure actuator.

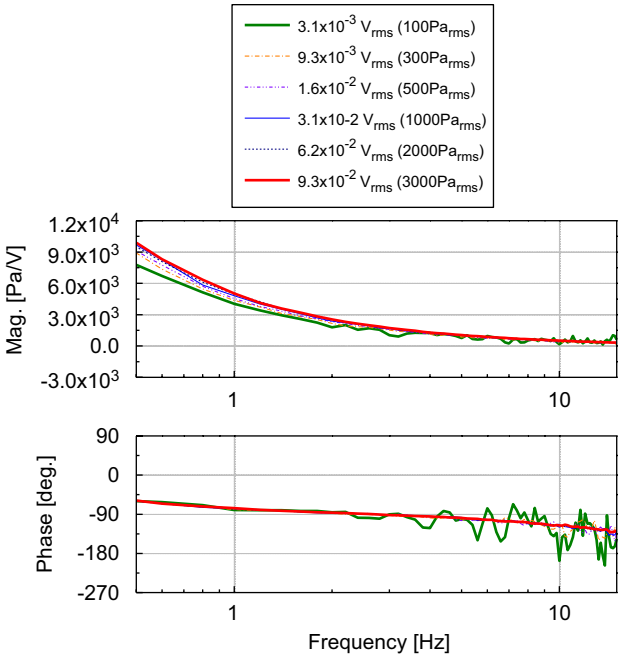


Fig. 7. Frequency response functions between input voltage to proportional valve and dynamic pressure in chamber: ————, root mean square value (r.m.s.) of input voltage (r.m.s. divided by static relationship between input voltage and chamber pressure, $3.1 \times 10^{-5}$ V/Pa) = $3.1 \times 10^{-3}\,V_{rms}$ ($100\,Pa_{rms}$); - - - - - - - -, $9.3 \times 10^{-3}\,V_{rms}$ ($300\,Pa_{rms}$); - · - · - · -, $1.6 \times 10^{-2}\,V_{rms}$ ($500\,Pa_{rms}$); ·····, $3.1 \times 10^{-2}\,V_{rms}$ ($1000\,Pa_{rms}$); - - - - - - -, $6.2 \times 10^{-2}\,V_{rms}$ ($2000\,Pa_{rms}$); and ═══, $9.3 \times 10^{-2}\,V_{rms}$ ($3000\,Pa_{rms}$).

Table 2
Proportional and derivative gains of feedback controller.

| Controller type | $K_p$ | $K_d$ |
|---|---|---|
| Controller gain | 15 | 0.1 |

where $V$ and $P$ denote the voltage into the valve and the pressure in chamber, respectively, and $G_{VV}$ and $G_{VP}$ are auto- and cross-power spectral density [14].

Fig. 7 shows results of $FRF_{VP}$ at various amplitudes of the random voltage inputs of $3.13 \times 10^{-3}$–$9.39 \times 10^{-2}\,V_{rms}$, which were processed by frequency resolution of 0.2 Hz, Hanning window, and 50 averaging. The frequency range of interest was set up to 0.5–15 Hz, which includes the fundamental natural frequency of the pneumatic vibration isolation Table 2 ~6 Hz. It seemed that the pressure actuator worked like a first order system with a very low cut-off frequency, implying that the response speed is too low to control the pressure properly in the chamber. Hence, in order to compensate for frequency response characteristics of the pneumatic actuator, both feedforward control and feedback control were used.

### 3.2.2. *Compensation of dynamic pressure actuator by feedforward and feedback control*

In order to compensate for the slow response characteristics of the valve-tube-chamber actuator by feedforward control, a mathematical model for the dynamic pressure actuator was required. Since it was not realistic to derive a mathematical model for the commercial valve due to insufficient information on geometric parameters and electromagnetic properties, measurements of the frequency response characteristics were simply curve fitted. Measurements and curves fitted by the first-order system in Eq. (14) at a given amplitude $3.13 \times 10^{-2}\,V_{rms}$ are shown in Fig. 8 [18].

$$G(j\omega) = \frac{P(j\omega),\ \text{measured pressure}}{V(j\omega),\ \text{input voltage}} = \frac{2.718 \times 10^4}{j\omega + 0.1045}. \tag{14}$$

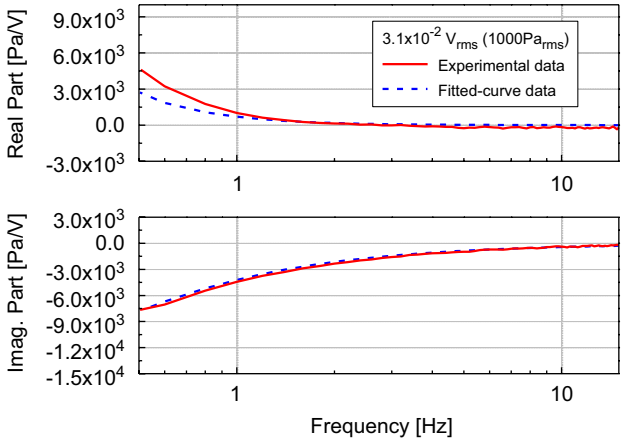


Fig. 8. Measurements and curve fitted results of pressure response characteristics of pneumatic actuator: ——, experimental results; and – – – -, fitted curve.

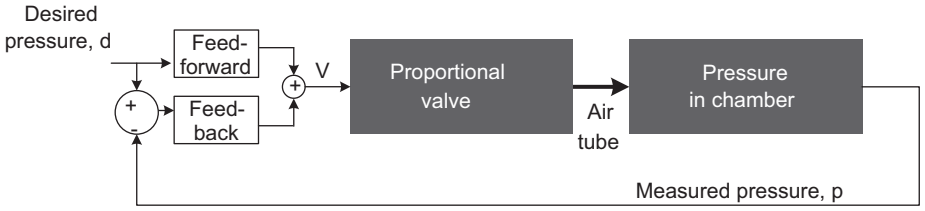


Fig. 9. Block diagram to control pneumatic pressure in chamber by both feedforward and feedback control.

Its inverse, $G^{-1}(j\omega)$, was then used to compute the voltage input to the valve for control of pressure in the chamber. Because the discrepancies between experimental measurements and predictions by the curve-fitted model were not negligible, particularly in the frequency range lower than 1 Hz, and furthermore amplitude dependence of the actuator frequency characteristics was observed, it was thought that use of feedforward control alone might not guarantee the desired performance of the actuator over the frequency range of interest. Therefore, a feedback PD controller with proportional and derivative gains described in Table 2 was added to the feedforward control mechanism:

$$u(t) = K_d\dot{e}(t) + K_p e(t),$$

$$e(t) = d(t) - p(t) \tag{15}$$

where $d(t)$ and $p(t)$ denote the desired pressure and the measured pressure, respectively, $u(t)$ is the feedback input voltage, $e(t)$ denotes the error between $d(t)$ and $p(t)$, $K_p$ and $K_d$ the proportional and derivative gain, respectively.

A block diagram for compensation of response characteristics of the valve actuator with the feedback and feedforward controllers is described in Fig. 9. Frequency response characteristics $\mathrm{FRD}_{DP}$ between desired random pressure and actual pressure in the chamber obtained by such compensations are plotted in Fig. 10 for three dynamic desired pressures of 1.6, 8.0, 80.0 $\mathrm{Pa_{rms}}$.

$$\mathrm{FRF}_{DP} = \frac{G_{DP}}{G_{DD}}, \tag{16}$$

where subscripts $D$ and $P$ denote desired and measured pressure, respectively [14]. Random signals up to 15 Hz for the desired pressure were generated by dSPACE ControlDesk & Simulink in MatLab. The generated and measured pressure signals were recorded by dSPACE (Model: ds1103). The control algorithm in Fig. 9 was

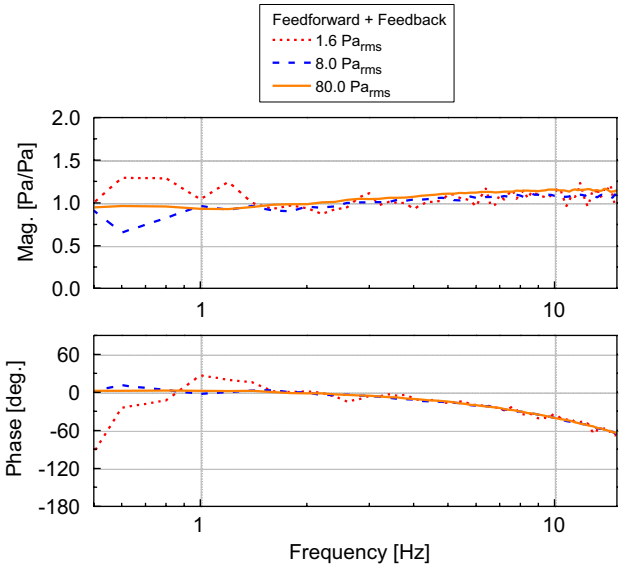


Fig. 10. Frequency response functions between desired pressure and feedback and feedforward controlled pneumatic pressure in chamber: ------, root mean square value of desired pressure = 1.6 Pa; – – –, 8.0 Pa; and ———, 80.0 Pa.

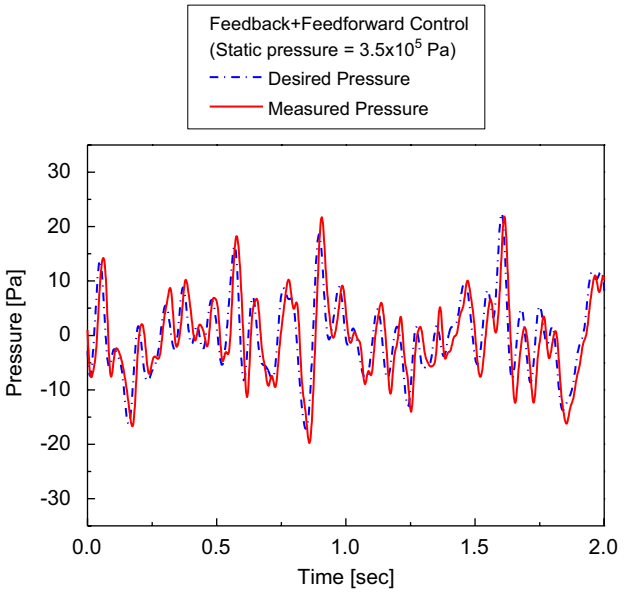


Fig. 11. Time domain response of feedback and feedforward controlled pneumatic pressure in chamber: — · — · —, desired pressure; and ————— , measured pressure.

also realized by dSPACE. The time domain signals for the amplitude of 8.0 $Pa_{rms}$ frequencies up to 15 Hz with sampling time of 0.001 s are shown in Fig. 11, where the pneumatic actuator works very well with just a small constant time delay of 0.013 s, which is thought small enough for the control of a plant with main dynamics at a few Hz. The constant time delay is computed from the frequency response characteristics $FRF_{DP}$ between desired and actual pressure in the chamber in Fig. 10 [14]. Because the phase of FRF is constantly decreased in Fig. 10, the delay time of actuator compensated by feedforward and feedback control could be computed by

$$\tau = \frac{\Delta\phi}{\Delta\omega} \cong 0.013\,\text{s}, \tag{17}$$

where $\tau$ denotes constant delayed time, $\Delta\psi$ difference of the phase between the desired and measured pressure in the frequency range of interest, $\Delta\omega$ difference between the upper and lower bound of the frequency range of interest.

Fig. 12 shows two FRFs between the desired and measured pressure; one by the feedforward control alone and the other by both feedforward and feedback control. It can be seen that, although the pressure is controlled well at frequencies higher than 3 Hz using the feedforward control alone, the phase distortion in the frequency range lower than 2 Hz is significant. Using the feedforward as well as feedback control algorithms, the response accuracy and speed could be assured down to the very small amplitude of pressure 1.6 $Pa_{rms}$ under the high static pressure of $3.5 \times 10^5$ Pa.

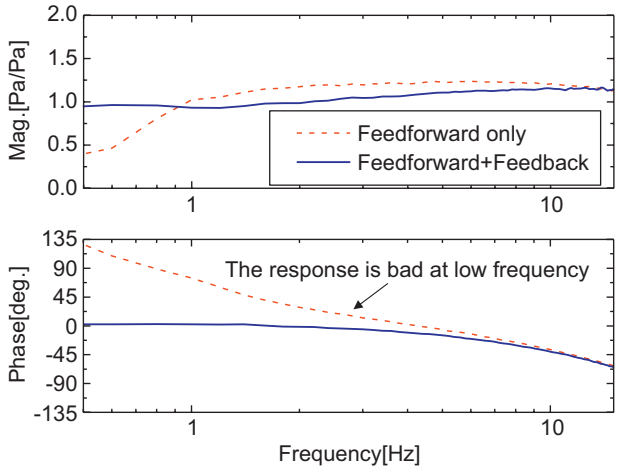


Fig. 12. Pressure response characteristics of pneumatic actuator with feedforward only and both feedforward and feedback control: ----, feedforward controller only; and ———, feedforward and feedback controller.


Fig. 13. Experimental set-up to measure transmissibility for base excitation.

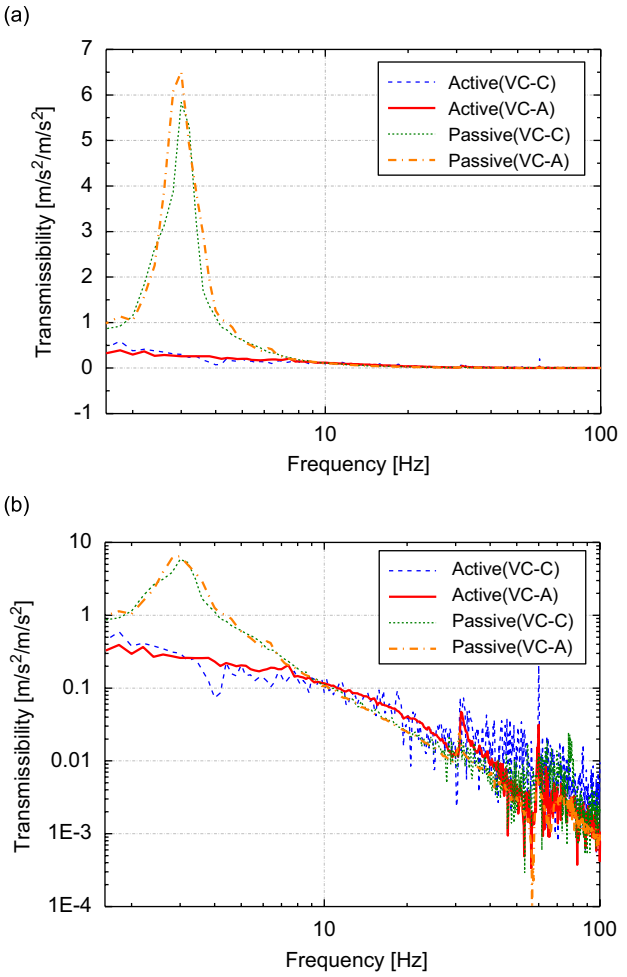


Fig. 14. Transmissibility of passive and actively controlled pneumatic vibration table: (a) linear scale; (b) log scale; - - - - - -, active one for VC-C ground vibration condition; ——————, active one for VC-A ground vibration condition; ····------····, passive one for VC-C ground vibration condition; and — - — - —, passive one for VC-A ground vibration condition.

### 3.3. *Experimental measurements on performance of active pneumatic vibration isolator for ground excitations*

Performance of the active pneumatic vibration isolator accomplished by the TDC technique and pressure actuator was measured in terms of transmissibility for ground excitations. The stable range for the tuning parameter observed from the experiment is expressed by Eq. (18). It shows somewhat difference compared with the theoretical range in Eq. (10) probably on account of measurement noise and/or unknown dynamics of the system.

$$15\,000 < b_{c\,\mathrm{exp}}^{+} < 35\,000 \tag{18}$$

The tuning parameter was chosen as the maximum value 35 000 in the stable range. The measurements were made and processed under the experimental conditions and the design parameters described in Section 3.1.

To show the enhancement of the isolation performance, transmissibility between the base and the payload was measured using two accelerometers, as shown in Fig. 13. High-sensitivity seismic accelerometers (model: PCB393B05, sensitivity: 10 V/g) were installed on the payload and the base and measured signals were post-processed to calculate the transmissibility, as described in Eq. (11). Transmissibility was estimated by applying Hanning window under ensemble average of 50 times, and observed with the frequency resolution of 0.2 Hz.

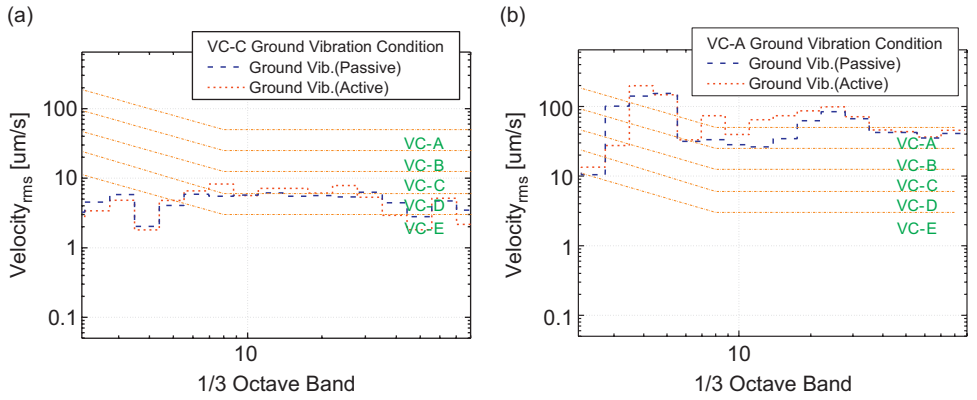


Fig. 15. $\frac{1}{3}$ Octave band analysis results for ground vibration of passive and active controlled system: (a) VC-C ground vibration; (b) VC-A ground vibration; – – –, vibration on floor (passive); and ------, vibration on floor (active).

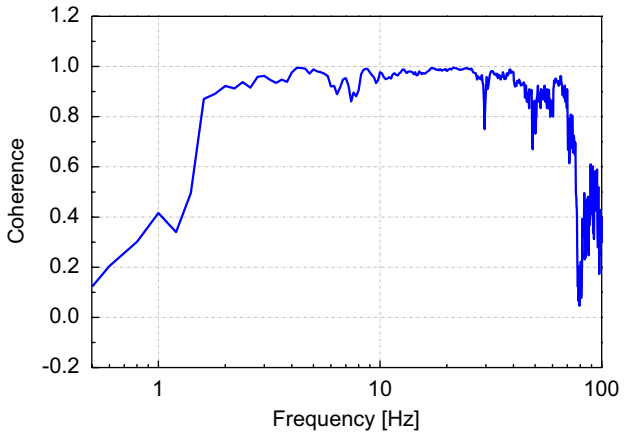


Fig. 16. Coherence between accelerations on payload and on base: ——, frequency range: 0.5–100 Hz, frequency resolution: 0.2 Hz, window: Hanning window, number of ensemble average: 50 times.

Fig. 14 shows the transmissibilities in linear and logarithmic scale between the base and the payload. 'VC-A' denotes a condition of ground vibration, in which two men ran near the isolator, of velocity magnitude 321 $\mu m/s_{rms}$ described as adequate in most instances for optical microscopes to 100 × and for other equipment of low sensitivity. 'VC-C' is another condition of ground vibration, where no one moved near the isolator, of velocity magnitude 23.0 $\mu m/s_{rms}$ described good for most demanding equipments including electron microscopes (TEMs and SEMs) and E-Beam systems [1]. Fig. 15 shows vibration criteria and spectrums of ground vibrations obtained using $\frac{1}{3}$ octave band analysis when transmissibility curves were to be measured. The lowest frequency of transmissibility curves shown in Fig. 14 is 1.4 Hz. Transmissibilities at lower than 1.4 Hz are not shown in the figure because the results are considered to be unreliable. One reason is the low coherence in that frequency range between two signals as shown in Fig. 16, probably due to insufficient input power. Another reason is that results of the transmissibility in case of passive isolators at some frequencies lower than the resonance frequency were greater than unity although, in theory, the transmissibility of a passive isolator must be greater than unity below the resonance frequency, meaning that something must have been wrong with experiments.

As shown in Fig. 14, transmissibilities of the active isolator were reduced clearly over the frequency range of main interest, i.e., lower than 10 Hz, compared with those of passive isolators. The root mean square value of transmissibility by the active isolator between 1.6 and 10 Hz is 0.21 while the one by the passive isolator is 1.95, meaning that the active isolator shows about 9.3 times better performance overall. Extending the highest

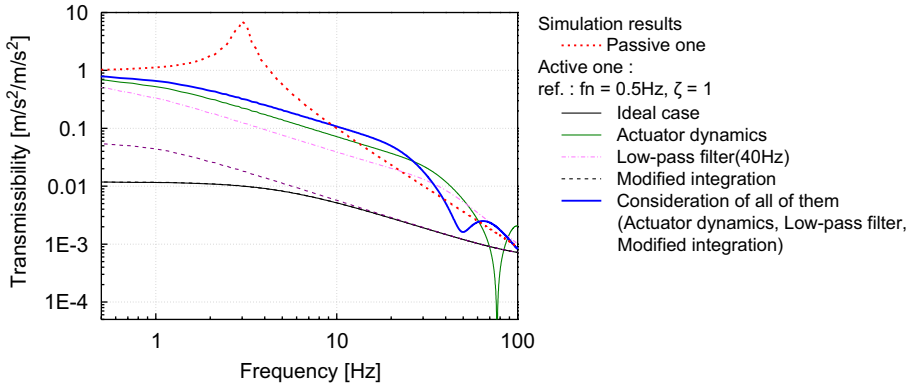


Fig. 17. Simulated transmissibilities under various simulation conditions: simulation results: ·····, passive one; ———, active one (ideal); ———, active one (consideration of actuator dynamics); ———, active one (low-pass filter (cut-off frequency = 40 Hz)); ------, active one (modified integration); and ———, active one (consideration of all these factors).

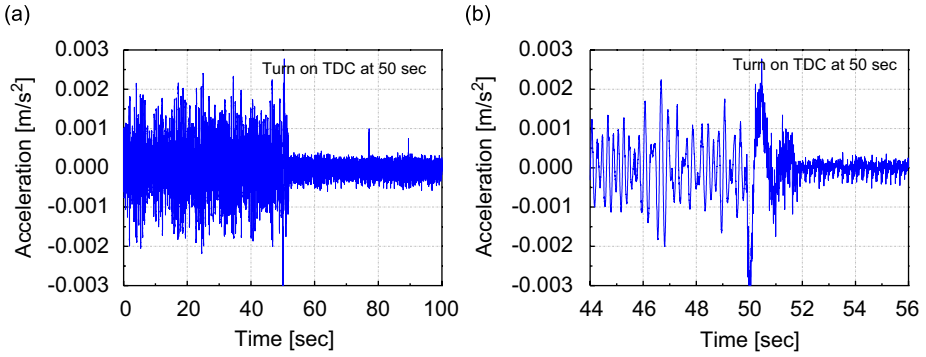


Fig. 18. Transient response of active pneumatic vibration isolator: (a) 0–100 s; (b) 44–56 s; and ———, start time delay controller at 50 s.

frequency of interest up to 100 Hz, the transmissibility in the actively controlled case is 0.07 while the one in the passive case is 0.58, meaning that the active isolator shows about 8.3 times better performance overall. Looking into the transmissibilities in more detail plotted in logarithmic scale in Fig. 14(b), it can be seen that the passive pneumatic isolator yielded slightly better performance relative to the active isolator over 10–40 Hz. The reason for this can be explained by the simulation results plotted in Fig. 17, where characteristics of the pneumatic actuator, low pass filter and modified integrator were taken into account.

All simulations were conducted for the VC-C ground vibrations of velocity magnitude 30 $\mu m/s_{rms}$. The transmissibilities were computed using the procedure described in Section 2.3. The state equation in Eq. (3) was used as the plant model, whose parameters are described in Table 1. The transmissibility of the passive isolator is very close to the experimental one, from the view point of the peak frequency near 3 Hz and the peak magnitude. Transmissibilities using the active isolator reflects several influences; each influence of the frequency response characteristics of the pneumatic actuator using feedforward and feedback control (constant time lag: 0.013 s), low-pass filter which is a second-order IIR filter (cut-off frequency of 40 Hz), modified integration, and all of these together. From this figure, the reason most responsible for the poor isolation performance above 10 Hz is believed to be the small time lag of the pneumatic actuator between the desired- and the measured-pressure in chamber.

Fig. 18 shows measurements of acceleration signals in time domain before and after power-on of the active controller for the excitation at VC-C. Duration of the transient region after power-on of the TDCler at 50 s is approximately 2 s, during which the main frequency component at 3 Hz, corresponding to the resonance of the passive pneumatic isolator, damps out.

## 4. Conclusion

In this paper, an active control methodology to enhance the isolation performance of pneumatic isolators in low frequency range is proposed. Application of what is referred to as time delay control law to the active air-pressure control is discussed. What the key problems are in the response speed and accuracy of the pneumatic actuator by is discussed and how to resolve the difficulty using the feedforward and feedback control theory is shown. Very excellent vibration isolation performance of the active isolator adapting the time delay control technique is shown through experiments not only over the main frequency range of interest lower than 10 Hz but also over a higher frequency range up to 100 Hz.

## Acknowledgments

This work has been financially supported by Basic Research Program of Korea Science and Engineering Foundation (R01-2006-000-10872-0), Development Program for Nanoscale Mechatronics of Korea Institute of Machinery and Materials, and BK21 of Ministry of Education.

## References

[1] C.G. Gordon, Generic vibration criteria for vibration-sensitive equipment, *Proceedings of SPIE*, San Jose, CA, 1999.
[2] C. Erin, B. Wilson, An improved model of the pneumatic vibration isolator: theory and experiment, *Journal of Sound and Vibration* 218 (1998) 81–101.
[3] J.H. Lee, K.J. Kim, Modeling of nonlinear complex stiffness of dual chamber pneumatic spring for precision vibration isolation, *Journal of Sound and Vibration* 301 (2007) 909–926.
[4] O. Makoto, I. Yoshiaki, S. Noboru, U. Kimio, Y. Hidetoshi, Active control for precision vibration isolation system, *Proceedings of First International Conference on Motion and Vibration Control*, 1992.
[5] I.-C. Shih, T.-Y. Wang, Design and adaptive control of a pneumatic vibration isolator, *Proceedings of International Conference of Motion and Vibration Control*, vol. 6(1), 2002, pp. 111–116.
[6] K. Kawashima, T. Kato, K. Sawamoto, T. Kagawa, Realization of virtual sub chamber on active controlled pneumatic isolation table with pressure differentiator, *Precision Engineering* 31 (2007) 139–145.
[7] J.-H. Song, K.-Y. Kim, Y.-P. Park, Active control of air-spring vibration isolator, *Korean Society of Mechanical Engineers* 19 (7) (1994) 1605–1617.
[8] S.-H. An, H.-S. Kim, K.-H. Riim, Active control of vibration isolation table using air-spring, *Korean Society for Noise and Vibration Engineering* 17 (7) (2007) 565–571.
[9] M. Yasuda, T. Osaka, M. Ikeda, Feedforward control of a vibration isolation system for disturbance suppression, *IEEE* 0-7803-3590-2 (1996) 1229–1233.
[10] K. Youcef-Toumi, O. Ito, A time delay controller for systems with unknown dynamics, *Journal of Dynamic Systems Measurement and Control* 112 (1990) 133–142.
[11] T.C. Hsia, L.S. Gao, Rubost manipulator control using decentralized linear time-invariant time-delayed joint controllers, *IEEE CH* 2876-1 (1990) 2070–2075.
[12] J.-W. Lee, P.-H. Chang, S.-H. Kim, A study on robust control of DC servo motor using time delay control and observer/controller stabilization, *Korean Society of Mechanical Engineers* 17 (5) (1993) 1029–1040.
[13] J.H. Lee, K.J. Kim, Computation of complex stiffness of inflated diaphragm in pneumatic springs by using FE codes, *Korean Society for Noise and Vibration Engineering* 16 (9) (2006) 919–925.
[14] J.S. Bendat, A.G. Piersol, *Random Data*, third ed., Wiley, New York, 2000.
[15] W.-H. Zhu, On active acceleration control of vibration isolation systems, *Proceedings of 43rd IEEE*, 2004.
[16] T.W. Parks, C.S. Burrus, *Digital Filter Design*, Wiley, New York, 1987.
[17] T. Wang, M. Cai, K. Kawashima, T. Kagawa, Modeling of a nozzle-flapper type pneumatic servo valve including the influence of flow force, *International Journal of Fluid Power* 6 (3) (2005) 33–43.
[18] *Optimization ToolBox$^{TM}$ 4 User's Guide*, The MathWorks, Inc., 2005.